Journal of Comparative Physiology B (2023) 193:425–438
https://doi.org/10.1007/s00360-023-01490-9

ORIGINAL PAPER

Gill surface area allometry does not constrain the body mass scaling of maximum oxygen uptake rate in the tidepool sculpin, *Oligocottus maculosus*

Derek A. Somo[1] · **Ken Chu**[1] · **Jeffrey G. Richards**[1]

Received: 5 July 2022 / Revised: 3 March 2023 / Accepted: 14 April 2023 / Published online: 7 May 2023

Abstract
The gill oxygen limitation hypothesis (GOLH) suggests that hypometric scaling of metabolic rate in fishes is a consequence of oxygen supply constraints imposed by the mismatched growth rates of gill surface area (a two-dimensional surface) and body mass (a three-dimensional volume). GOLH may, therefore, explain the size-dependent spatial distribution of fish in temperature- and oxygen-variable environments through size-dependent respiratory capacity, but this question is unstudied. We tested GOLH in the tidepool sculpin, *Oligocottus maculosus*, a species in which body mass decreases with increasing temperature- and oxygen-variability in the intertidal, a pattern consistent with GOLH. We statistically evaluated support for GOLH versus distributed control of $\dot{M}o_2$ allometry by comparing scaling coefficients for gill surface area, standard and maximum $\dot{M}o_2$ ($\dot{M}o_{2,Standard}$ and $\dot{M}o_{2,Max}$, respectively), ventricle mass, hematocrit, and metabolic enzyme activities in white muscle. To empirically evaluate whether there is a proximate constraint on oxygen supply capacity with increasing body mass, we measured $\dot{M}o_{2,Max}$ across a range of Po_2s from normoxia to P_{crit}, calculated the regulation value (R), a measure of oxyregulatory capacity, and analyzed the R-body mass relationship. In contrast with GOLH, gill surface area scaling either matched or was more than sufficient to meet $\dot{M}o_2$ demands with increasing body mass and R did not change with body mass. Ventricle mass ($b = 1.22$) scaled similarly to $\dot{M}o_{2,Max}$ ($b = 1.18$) suggesting a possible role for the heart in the scaling of $\dot{M}o_{2,Max}$. Together our results do not support GOLH as a mechanism structuring the distribution of *O. maculosus* and suggest distributed control of oxyregulatory capacity.

Keywords Gill surface area · Metabolic scaling · Respiratory capacity · Oxyregulation · Intertidal fish · Gill oxygen limitation theory · Oxygen uptake capacity · Anatomical gill scaling · Hypoxia · Tidepool fish

Introduction

The recently resurgent gill oxygen limitation hypothesis (GOLH) posits that the intraspecific allometry of whole-organism metabolic rate in fish is a consequence of the "dimensional tension" between the growth of the essentially two-dimensional oxygen exchange surface (e.g., gill surface) and the three-dimensional oxygen-consuming body volume (Pauly 2021). Specifically, GOLH suggests that slower growth of the oxygen exchange surface (i.e., gills in fishes) directly limits the oxygen consumption rate of the body, producing hypometric scaling of both metabolic rate and growth (Pauly 2021). Since warming generally increases oxygen demand exponentially in ectotherms ($Q_{10} \sim 2$–3, (Clarke 2017)), GOLH has also been suggested to underlie the decline in maximum body size of fish with marine and freshwater warming by exacerbating the hypothesized morphological limitation on oxygen uptake capacity at the gills (Cheung et al. 2013; Cheung and Pauly 2016). Perversely, as oxygen demands in marine ectotherms increase with warming, ocean oxygen content is declining (Gattuso et al. 2015). Hypoxia associated with ocean warming and, at more local scales, eutrophication, can impose an environmental constraint on the ability of marine ectotherms to meet their metabolic oxygen needs (Farrell and Richards 2009; Ern 2019; Pörtner 2021; Rodgers 2021). GOLH's hypothesized gill morphology constraint on oxygen uptake capacity and

Communicated by B. Pelster.

✉ Derek A. Somo
derek.somo@gmail.com

[1] Department of Zoology, The University of British Columbia, Vancouver, BC V6T 1Z4, Canada

growth may, therefore, mediate the effects of both ocean warming and deoxygenation on marine ectotherm growth and maximum body size in the multiple-stressor environment imposed by climate change.

There is considerable debate over the physiological validity of GOLH, particularly as a mechanism setting the allometry of oxygen uptake rate ($\dot{M}o_2$) and metabolic rate with body size (Lefevre et al. 2017, 2018, 2021; Pauly and Cheung 2018a, b; Pauly 2021). A major source of contention is the implication of GOLH that control of oxygen uptake and consumption is vested in a single, morphometric control locus, the gill gas exchange surface area (Scheuffele et al. 2021). This contrasts with empirical evidence for distributed control of oxygen uptake and consumption among several steps in the oxygen transport cascade as well as oxygen and ATP demand, with metabolic state (i.e., basal/standard or maximal) also being a key determinant of control distribution (Darveau et al. 2002; Hochachka et al. 2003; Weibel and Hoppeler 2005). Resolving whether GOLH provides an accurate mechanistic basis for environmental impacts on fish metabolism and growth is key to accurately projecting ocean warming and deoxygenation impacts on fisheries and marine ecosystem functioning.

The debate over GOLH has largely involved theoretical analyses of published intraspecific scaling coefficients for gill surface area, oxygen uptake rate, and growth, but few empirical data exist to directly test GOLH's proposed gill limitation of oxygen uptake rate. In a recent test of GOLH predictions, Scheuffele et al. (2021) calculated the ratio of gill surface area to both standard $\dot{M}o_2$ ($\dot{M}o_{2,Standard}$) and maximum normoxic $\dot{M}o_2$ ($\dot{M}o_{2,Max}$). The authors analyzed the body mass scaling relationship of this ratio, termed the *S* ratio, and predicted that a scaling coefficient for *S*, $b_S, < 0$ would be consistent with GOLH while $b_S \geq 0$ implies that gill surface area growth is sufficient or in excess of that required to support increases in oxygen uptake rate as individuals reach larger body sizes, refuting GOLH. Although Scheuffele et al. (2021) concluded that the available data do not support a gill surface area limitation on oxygen fluxes with increasing size, data for testing *S* at $\dot{M}o_{2,Standard}$ were available for only nine species and *S* for $\dot{M}o_{2,Max}$ for three species, indicating the need for more data to determine the generality of their conclusions.

Beyond the impacts of ocean warming and deoxygenation with climate change, if GOLH is a ubiquitous driver of fish metabolic rate and growth, GOLH may provide a key physiological mechanism structuring the size distribution of species living in marine habitats with variable temperature and oxygen regimes. Intertidal rock pools vary dramatically in temperature, oxygen, carbon dioxide, and pH with the daily ebb and flow of the tides (Truchot and Duhamel-Jouve 1980). Pools emersed at low tide can quickly warm during the day and become hyperoxic, hypocarbic, and alkaline with high photosynthetic activity while nocturnal respiration reverses these conditions leaving pools hypoxic, hypercarbic, and acidic (Richards 2011). The degree of variation in abiotic environmental parameters such as temperature and oxygen generally directly varies with vertical elevation of pools above the low water mark, although other physical and biological characteristics, including pool depth and volume, algal cover, rugosity, and angle of insolation, can dramatically reduce the strength of the direct relationship between vertical elevation above the low water mark and abiotic pool condition variability (Metaxas and Scheibling 1993; Zander et al. 1999; Wuitchik et al. 2018). Although the ecological literature demonstrates that each of the above factors can contribute to the age and size structure of populations among rock pools, organisms living in rock pools often show an intraspecific small-to-large body size distribution that correlates with the degree of environmental variability among pools (Nakamura 1976; Metaxas and Scheibling 1993; Wuitchik et al. 2018). Such an intraspecific spatial distribution of body sizes is consistent with a GOLH-derived growth limitation in abiotically variable tidepools, but the role of gill surface area in setting whole-organism respiratory and metabolic capacity at different body sizes in intertidal fishes remains unstudied.

The tidepool sculpin (*Oligocottus maculosus*) is a useful model for studying the potential for GOLH to structure the size-dependent spatial distribution of fish in temperature- and oxygen-variable environments. Tidepool sculpins are an abundant tidepool resident species that preferentially inhabits rocky tidepools in the mid-to-upper intertidal on the Pacific coast of North America, ranging from central California to Alaska (Froese and Pauly 2021). A previous analysis demonstrated that smaller adult and juvenile individual *O. maculosus* occupy smaller, warmer pools while larger adults occupy larger, cooler pools (Wuitchik et al. 2018). Although Wuitchik et al. (2018) did not analyze oxygen variability in their analysis, the temperature variation they observed likely correlates with oxygen variation as has been previously demonstrated in *O. maculosus* habitat (Richards 2011).

Our objective was to investigate whether GOLH may contribute to the size-dependent spatial distribution of a tidepool resident fish species, the tidepool sculpin (*Oligocottus maculosus*). We analyzed the body mass scaling relationships of normoxic $\dot{M}o_{2,Max}$, $\dot{M}o_{2,Standard}$, and gill surface area using the *S* ratio and b_S analysis developed by Scheuffele et al (2021). To determine whether body mass scaling of other aspects of oxygen supply and demand might contribute to setting body size scaling of whole-organism $\dot{M}o_{2,Max}$, we analyzed the body mass scaling of ventricle mass, hematocrit, and muscle metabolic enzyme activities. We focused on the scaling of white muscle metabolic enzymes given that this tissue makes up a large proportion of body mass,

underlies the exhaustive burst swimming this species performs during exhaustive chases, and the minimal content of red muscle in this benthic, generally sluggish species. To empirically evaluate whether there is a proximate constraint on oxygen uptake capacity with increasing body size in *O. maculosus*, we measured $\dot{M}o_{2,Max}$ across a range of Po_2s from normoxia to the critical Po_2 for $\dot{M}o_{2,Standard}$ (P_{crit}). We used the $\dot{M}o_{2,Max}$ vs. Po_2 data to calculate the regulation value (Alexander Jr. and McMahon 2004) as a metric for evaluating the effect of body mass on oxyregulatory capacity. If the size-structured spatial distribution of *O. maculosus* is a consequence of the GOLH mechanism, we would predict that gill surface area scales hypometrically with body mass, and both $\dot{M}o_{2,Max}$ and $\dot{M}o_{2,Standard}$ would scale with exponents less than the scaling exponent of gill surface area, i.e., $b_S < 0$, for both normoxic $\dot{M}o_{2,Max}$ and $\dot{M}o_{2,Standard}$. As GOLH assumes there is a proximate constraint on oxygen uptake capacity with increasing body size, we predicted that R would decrease with increasing body mass and that P_{crit} would increase with increasing body mass, both of which would indicate a declining oxyregulatory capacity with increasing body size. Finally, we predicted based on GOLH that other aspects of oxygen supply and demand would either have no relationship with body mass (e.g., hematocrit, (Calder 1996)) or would have scaling exponents greater than the scaling exponent for gill surface area, indicating excess capacity relative to gill surface area and, therefore, no contribution to setting the scaling of oxygen uptake capacity.

Materials and methods

Animal collection and housing

Tidepool sculpins (*O. maculosus*) were collected under Department of Fisheries and Oceans Canada permit XR 239 2017 and Huu-Ay-Aht Heritage Investigations permit HFN 2017-027 in September 2017 from rocky intertidal pools and the shallow subtidal on Wizard Islet and Ross Islet near Bamfield Marine Sciences Centre (British Columbia, Canada, 48.8355° N, 125.1355° W). Fish in tidepools were collected using dipnets and minnow traps, and a pole-seine net was used to collect larger individuals from eelgrass and sandy substrate in the shallow subtidal (< 1 m depth) adjacent to intertidal pools. As recommended for analyses of GOLH (Pauly 2021), the body mass range of fish collected spanned from the largest fish we could obtain, which was similar to the largest documented body size for *O. maculosus* (~ 10 g, (Froese and Pauly 2021)), down to approximately one-third of the maximum size of fish collected, with a final range from ~ 3.5 to 10 g. Animals were transported to The University of British Columbia (UBC) and housed in a recirculation system with aerated 35‰ artificial seawater (Instant Ocean, Blacksburg, VA, USA) at 12 °C with a 12L:12D photoperiod until respirometry experiments were run from November 2018 through January 2019, when fish were terminally sampled for tissue analyses. Fish were fed ad libitum three times per week on a diet of Antarctic krill, spirulina-fed brine shrimp, and blood worms.

To facilitate identification of individual fish and avoid aggressive interactions between large and small individuals, fish were separated into groups of 4–5 individuals of roughly similar size and held in separate buckets within the acclimation tank. The buckets had mesh windows to allow water exchange with the greater acclimation tank water volume and environmental enrichment simulating a rocky, eelgrass habitat. Fish within each bucket received a unique tail fin clip pattern, which together with their holding bucket identity was used to uniquely identify each fish. Exhaustive chases and respirometry measurements were performed at 12.0 ± 0.1 °C (Target temperature ± observed range, Table S1). Every phenotype was measured in every fish, resulting in a sample size $N = 17$ for every trait except ventricle dry mass, with $N = 15$ due to sample loss.

All experimental procedures were approved by the UBC Animal Care Committee (A17-0293).

Experimental protocols

Respirometry

Respirometry details recommended for reporting to improve reproducibility (Killen et al. 2021) are given in Table S1. $\dot{M}o_{2,Max}$ and P_{crit} data were collected using closed respirometry, and $\dot{M}o_{2,Standard}$ data were collected using intermittent respirometry. For all respirometry experiments, glass respirometers with a ratio of body mass (g): respirometer volume (mL) at ~ 1:15 (range of ratios: [7.1, 37], Table S1) were submerged in a temperature-controlled water bath and connected to flush pumps (EXT Inline pump, Cobalt Aquatics, Rock Hill, SC, USA). Flushing and closed periods during intermittent respirometry trials were controlled via a USB power switch (model Cleware 1 USB-SwitchC IEC 16A Product no.:24-1, Cleware GmbH, Germany) using Aquaresp v 3.0 software (AquaResp.com). Bath temperature was monitored using a digital temperature probe (catalog no. 11-463-47A, Fisher Scientific, Waltham, MA, USA). The temperature of the bath was regulated using a benchtop temperature regulator (model 1160S, VWR International, Radnor, PA, USA) connected to a water-filled stainless-steel heat-exchange coil submerged in the bath. Additional flushing pumps circulated bath water to ensure a uniform temperature. For normoxic experiments, bath oxygen levels were maintained above ~ 80% air saturation (see Table S1 for details) using air stones connected to an aquarium air

pump. Specific levels of hypoxia in hypoxic $\dot{M}o_{2,Max}$ trials were achieved by adding nitrogen from an industrial gas cylinder (Praxair, Vancouver, BC, Canada) through an air stone and manually adjusting flow via a regulator. Po_2 (in % air saturation units, % air sat.) in the bath and respirometers was sampled every 10 s using a fluorescent probe connected to a benchtop spectrophotometer by a fiber optic cable (FOXY system, Ocean Optics, Dunedin, FL, USA) and recorded using Ocean Optics' software (Neofox Viewer v2.0). A probe was inserted through a rubber stopper on the top of each respirometer. A plastic mesh cage excluded fish from interacting with the probe. Water in respirometers was mixed during closed periods using a magnetic stir bar placed under a rigid plastic mesh false bottom, with a magnetic stir plate positioned under the respirometry bath.

Normoxic and hypoxic $\dot{M}o_{2,Max}$ estimates were obtained using an exhaustive chase protocol and closed respirometry. An individual fish was placed in a bucket of normoxic acclimation-tank water at acclimation temperature and manually chased to exhaustion. A fish was considered exhausted if it failed to respond to a tail pinch and failed to immediately right itself after being turned ventral-side up. The exhausted fish was immediately placed in a glass respirometer submerged in the respirometry bath at the target oxygen level. $\dot{M}o_{2,Max}$ data were collected for each fish at 5 oxygen levels: 100% air sat. (i.e., normoxic $\dot{M}o_{2,Max}$, mean trial DO > ~90% air sat.), 80% air sat., 60% air sat., 40% air sat., and 20% air sat. To minimize the effect of order of oxygen treatment on our analysis, after collecting normoxic $\dot{M}o_{2,Max}$ data for all fish first, we haphazardly assigned the order of oxygen treatments for each group of fish (see "Animal collection and housing"). For normoxic $\dot{M}o_{2,Max}$, the respirometer and recirculation bath were at 100% air saturation when the respirometer was sealed to start recording $\dot{M}o_2$. For every other oxygen level, the respirometry bath and respirometer were held ~ 2–5% air sat. above the target level until the exhausted fish was placed in the respirometer and the fish allowed to draw the oxygen down until the respirometer was at ~ 2–5% air sat. below the target level. This method ensured the mean Po_2 experienced during the trial was equal to the target Po_2. Fish were weighed immediately following each respirometry trial prior to being returned to their respective holding buckets within the acclimation tank for recovery. Fish were recovered for a minimum of 3 days between $\dot{M}o_{2,Max}$ trials with 1 feeding to satiation on the first day of recovery followed by 2 days of fasted recovery.

After collecting $\dot{M}o_{2,Max}$ data for every fish at 20%, 40%, 60%, 80% and 100% air sat., fish were recovered for at least 1 week, with a feeding 1 day prior to 2 days of fasting before collecting $\dot{M}o_{2,Standard}$ and P_{crit} data. $\dot{M}o_{2,Standard}$ data were collected using intermittent respirometry followed by a closed-style P_{crit} trial in which the respirometer was sealed and a progressive hypoxia exposure imposed by the fish consuming oxygen. During $\dot{M}o_{2,Standard}$ trials, flushing and closed period durations were adjusted for each trial to ensure a minimum of 5 min of linear decline in respirometer Po_2 during closed periods and sufficient time to reoxygenate the respirometer to dissolved oxygen (DO) levels > 95% air sat. during flushing periods, typically 5–10 min. Visual disturbance of the fish was prevented by covering the bath with black plastic, but the placement of the plastic still allowed light to reach the fish so they continued to experience the acclimation photoperiod throughout the respirometry trials. $\dot{M}o_2$ data for $\dot{M}o_{2,Standard}$ estimation were collected over a 48 h period. At the end of the $\dot{M}o_{2,Standard}$ trial period, to begin the P_{crit} portion of a trial, flush pumps were manually powered off and the fish allowed to consume the oxygen contained in the respirometer until changes in oxygen tension in the respirometer over a 5 min period could not be visually detected on the NeoFox graphical user interface. Fish maintained ventilatory movements and did not lose equilibrium during P_{crit} trials using this protocol. Fish were weighed immediately following the end of the $\dot{M}o_{2,Standard}$–P_{crit} trial and returned to their holding buckets in the acclimation tank for recovery for 1 week with a regular feeding schedule before terminal sampling for tissue analyses.

The water bath, respirometers, and associated tubing were bleached daily following $\dot{M}o_{2,Max}$ trials or in between each set of concomitant $\dot{M}o_{2,Standard}$–P_{crit} trials using a 10% hypochlorite solution for 30 min to minimize background respiration. Although we did not measure background respiration in this study, we used data from a nearly concomitant study in *O. maculosus* using the same respirometry system and a comparable mass range (Somo et al. 2022) to determine that background respiration was likely sufficiently low to not impact our current analysis and conclusions (supplemental materials and methods).

Conversion of raw respirometry data to $\dot{M}o_2$ values

Recorded percent air saturation values were converted to Po_2 in kPa using local reported barometric pressure measurements at the nearest Department of Environment and Natural Resources Canada weather station (49° 11′ 41″ N, 123° 11′ 2″ W) and assuming an atmospheric oxygen fraction of 0.2095. Po_2 was converted to µmol O_2 using salinity- and temperature-appropriate solubility coefficients from Boutilier et al. (1984) and the volume of the respirometer less the volume of the fish, with an assumed fish density of 1 mL g^{-1}.

Calculation of $\dot{M}o_{2,Max}$, $\dot{M}o_{2,Standard}$, and P_{crit} estimates

$\dot{M}o_{2,Max}$ estimates were obtained following the rolling regression method of Prinzing et al. (2021). Briefly, for each $\dot{M}o_{2,Max}$ trial at each Po_2, we obtained rolling ordinary least squares regressions over the full measurement period using the "roll_regress()" function from the rollRegres package (Christoffersen 2019) as implemented in the supplemental R code in Prinzing et al. (2021). This function yields a dataset of regression coefficients from which we could select the steepest slope (i.e., largest regression coefficient) as our estimate of $\dot{M}o_{2,Max}$ for a given regression window width. We obtained $\dot{M}o_{2,Max}$ estimates for window widths of 1 min, 2 min, 3 min, 4 min, and 5 min. We then plotted each regression associated with the $\dot{M}o_{2,Max}$ slope from each window width over the raw $\dot{M}o_2$ data for each trial and, for each experimental % air sat. treatment, visually determined the shortest window width for which a reasonable, consistent estimate of $\dot{M}o_{2,Max}$ could be obtained (Fig S1). We used a final window width of 80 s for estimating $\dot{M}o_{2,Max}$ at 100% air sat. and a 2 min window width for all other treatments (i.e., $\dot{M}o_{2,Max}$ at 20% air sat.—80% air sat.).

$\dot{M}o_2$ values during $\dot{M}o_{2,Standard}$ trials were calculated from each "closed period" using a minimum of 300 s of the most linear portion of the slope ($R^2 \geq 0.9$) using Labchart Reader v8.1.9 (ADInstruments Inc., Colorado Springs, CO, USA). $\dot{M}o_2$ values during P_{crit} trials were obtained using end-to-end 300 s linear regressions in Labchart Reader software. $\dot{M}o_{2,Standard}$ and P_{crit} were estimated as described in (Chabot et al. 2016) and (Claireaux and Chabot 2016), respectively. The first 5 h of $\dot{M}o_2$ data, which generally accounted for the decline in $\dot{M}o_2$ associated with recovery from handling, were discarded and the remaining data grouped into normal distributions (maximum of 4) using clustering analysis via the "calcSMR" function of the R package "fishMO$_2$" (Chabot 2020). As recommended by Chabot et al. (2016), $\dot{M}o_{2,Standard}$ was estimated as the mean of the lowest normal distribution when the coefficient of variation of the $\dot{M}o_2$ data was less than 5.4%; otherwise $\dot{M}o_{2,Standard}$ was estimated as the quantile $P = 0.2$ of the $\dot{M}o_2$ data post-handling recovery. P_{crit} was estimated as the intersection of estimated $\dot{M}o_{2,Standard}$ and the regression of data in the oxyconforming range of oxygen tensions using the "calcO$_2$crit" function (R package "fishMO$_2$", (Chabot 2020)).

Calculation of regulation value

Originally proposed by Alexander Jr. and McMahon (2004), the regulation value R provides an index of the capacity to regulate $\dot{M}o_2$ in hypoxia. The regulation value R is calculated as the percentage of the area under the curve for a hypothetical "perfect regulator" occupied by the area under the curve of experimentally obtained $\dot{M}o_2$ data (Fig. 2a), with $\dot{M}o_2$ normalized to $\dot{M}o_{2,Max}$ (Fig. 2b). A perfect regulator would have an R value of 100%, perfect conformer would have an R value of 50%, with increasing degrees of regulatory capacity above 50% and hypersensitivity to mild hypoxia indicated by R values below 50%. Importantly, the regulation value, unlike other analytical approaches such as the regulation index (Mueller and Seymour 2011), is agnostic about whether and what kind of continuous function and physiological mechanisms underlie the $\dot{M}o_{2,max}$–Po_2 relationship. There is lively debate and ongoing investigation into the nature and physiological basis of the continuous relationship between $\dot{M}o_2$ and Po_2 (Farrell et al. 2021; Seibel et al. 2021a; Zhang et al. 2022), so the regulation value provides a means of empirically describing whole-organism regulatory capacity without assuming a specific physiological basis for empirically observed regulatory capacity.

The regulation value R was calculated for each individual by first normalizing each $\dot{M}o_2$ value to the maximum $\dot{M}o_2$ for that individual irrespective of Po_2 (Fig. 2b, c). Po_2 was converted to percent air saturation units (% air sat.) and R was calculated as:

$$R = \frac{\sum_{P_{crit}}^{100\%\text{AirSat}} \left(W \times \dot{M}o_{2,Obs}\right)}{\sum_{P_{crit}}^{100\%\text{AirSat}} \left(W \times \dot{M}o_{2,PR}\right)} \times 100\%,$$

where W is the width (5% air sat., Alexander Jr. and McMahon 2004) and $\dot{M}o_{2,Obs}$ is the height of a rectangle describing the observed, normalized $\dot{M}o_{2,Max}$ at a given Po_2 of either P_{crit}, 20% air sat., 40% air sat., 60% air sat., 80% air sat., or 100% air sat., and $\dot{M}o_{2,PR}$ is the normalized max at the same Po_2 for a perfect regulator, i.e., $\dot{M}o_{2,PR} = 100\%$. Note that P_{crit} in *O. maculosus* indicates the threshold at which maximum respiratory capacity cannot support $\dot{M}o_2 > \dot{M}o_{2,Standard}$, i.e., absolute aerobic scope = 0 (Somo et al. 2022).

Tissue sampling

Fish were recovered for at least 1 week following the conclusion of respirometry during which they were fed on their regular schedule. The evening before sampling the fish were placed in containers with a 1 L bottom and mesh windows above to allow water exchange with the surrounding home acclimation aquarium in which the sampling containers were placed. The next morning, the fish were isolated into the 1 L bottom basin by gently lifting the sampling container out of the acclimation aquarium and unobtrusively anaesthetized with the addition of an overdose of benzocaine (250 mg L^{-1},

Sigma-Aldrich, USA) to the sampling container. Benzocaine may acutely elevate hematocrit in fish, (e.g., Phuong et al. 2017; Soivio et al. 1977), but such an effect should support our analysis of the maximum capacity for oxygen uptake given the increase in hematocrit associated with splenic release during exercise (Gallaugher and Farrell 1998). Fish were fully anaesthetized within 1 min of exposure, and blood was sampled after removing fish from the anaesthestic bath via caudal severance. Blood was collected into a heparinized capillary tube and used for hematocrit measurements. The trunk was then cut just posterior to the anus and then cut in half dorsoventrally, avoiding the spine, to expose white muscle. The sectioned trunk was then wrapped in aluminum foil and flash frozen in liquid nitrogen. The heart was then removed, wrapped in aluminum foil, and flash frozen in liquid nitrogen. The right gill basket was dissected out, cleaned of excess cartilage and skin, preserved in Karnovsky's fixative (1% glutaraldehyde, 1% formaldehyde in a phosphate buffer, (Karnovsky 1965)) and refrigerated at 8 °C until further analysis.

Hematocrit analysis

After sampling, blood sample capillary tubes were sealed and immediately centrifuged at 5000×*g* for 3 min. Hematocrit was calculated as $\mathrm{Hct} = (\mathrm{R/T}) \times 100\%$, where R is the measured height of the capillary tube occupied by packed red blood cells divided by T, the total measured height of the blood sample.

Gill surface area analysis

Gill surface area was measured following Henriksson et al. (2008). The total number of filaments on each gill arch was counted under a stereomicroscope (Olympus SZX10), and the length of every fifth filament was measured using digital image capture and software (light: LED transmitted light, halogen reflected light; camera: Olympus DP72 digital camera, 4140 × 3096 pixels, 12 bits, high sensitivity up to ISO1600; software: Olympus cellSense standard software, Tokyo, Japan). The linear spacing between lamellae along each filament was measured over 10 lamellae at the base, mid-section, and tip of every fifth filament on the first gill arch. Serial cross sections of every fifth filament of the first gill arch were performed with a razor blade under the stereomicroscope, and lamellar area was quantified on at least 3 lamellae per filament region (base, mid-section, tip) per filament using cellSense software. Total gill surface area was calculated as $A = L_F N_L B$, where L_F is the total filament length (mm) on all gill arches, N_L is the number of lamellae per millimeter on both sides of the filament, and B is the average bilateral surface area of the lamellae (mm^2).

Ventricle dry mass analysis

Heart samples were thawed and the ventricle separated out under a stereomicroscope. Each ventricle was briefly and gently blotted on a kimwipe, placed in a pre-weighed aluminum weighing boat (Sigma-Aldrich), dried at 55 °C for 72 h, and then weighed after bringing the boats to room temperature. Mass measurements were taken using a micro balance (XPR2, Mettler Toledo, Mississauga, Ontario, Canada). Ventricle dry mass was calculated as $M_V = M_{BV} - M_B$, where M_V, the ventricle dry mass, is the difference between the pre-weighed boat mass (M_B) and the post-drying boat mass + ventricle (M_{BV}).

White muscle enzyme activity analysis

Frozen white muscle samples were broken into chunks in a liquid nitrogen-cooled mortar and pestle and any skin tissue was removed before crushing and powdering the sample. Approximately 80–100 mg of powdered white muscle was added at a ratio of 1 mg:5 µL homogenization buffer (in mM at pH 7.2: 25 mM K_2HPO_4, 5 mM $MgCl_2 \cdot 6H_2O$) then immediately sonicated on ice in 3–10 s bursts using a Kontes Micro Ultrasonic Cell Disrupter (Kontes, Vineland, NJ) on its highest setting. The homogenate was centrifuged at 600×*g* at 4 °C for 10 min, the supernatant was transferred and centrifuged again at 600×*g* at 4 °C and the supernatant was aliquoted and frozen at − 80 °C until enzyme activity and protein content analyses.

Maximal enzyme activities were determined spectrophotometrically (VersaMax, Molecular Devices, Sunnyvale, CA) by measuring the disappearance of nicotinamide adenine dinucleotide (NADH) at 340 nm (LDH) over a 10-min incubation period, the appearance of 5-thio-2-nitrobenzoic acid (TNB) as a result of the reaction of free CoA with 5,5′-dithiobis(2-nitro-benzoic acid) (DNTB) at 412 nm (CS) over a 10-min incubation period, and the disappearance of reduced cytochrome C at 550 nm (COX) over a 3-min incubation period. The assay conditions were as follows: (in mM): LDH = 50 Tris at pH 7.4, 2.5 pyruvate, 0.6 NADH; CS = 50 Tris at pH 8.0, 0.5 oxaloacetate, 0.3 acetyl-CoA, 0.15 5,5dithiobis-2-nitrobenzoic acid; COX = 25 K_2HPO_4 at pH 7.2, 5 $MgCl_2$, 0.6 lauryl maltoside, 0.05 reduced cytochrome C. Reaction substrates such as pyruvate (LDH), oxaloacetate (CS), and reduced cytochrome C (COX) were at saturating levels. We used empirically determined extinction coefficients to calculate maximal enzyme activities. Total soluble protein was determined in each homogenate using the Bradford protein assay (Bradford 1976). Maximum enzyme activities were normalized to total soluble protein and grams of wet tissue, and maximum COX activity was

also normalized against maximum CS activity as an index of maximum COX activity relative to mitochondrial density.

Statistical analyses

All statistical analyses were performed in R v 4.0.0 "arbor day" (R Core Team 2020).

The S ratio, developed by Scheuffele et al. (2021), is a metric quantifying the relationship described by Pauly (2021) between the relative oxygen supply, or gas exchange surface area available for a given oxygen uptake rate (e.g., $\dot{M}o_{2,Max}$ or $\dot{M}o_{2,Standard}$), and body size. *S* ratios for both $\dot{M}o_{2,Max}$ in normoxia (S_{MMR}) and $\dot{M}o_{2,Standard}$ (S_{SMR}) were calculated by dividing each individual's measured gill surface area (in mm^2) by that individual's normoxic $\dot{M}o_{2,Max}$ or $\dot{M}o_{2,Standard}$ (in µmol O_2 per h).

All phenotypic data were natural-logarithm transformed prior to fitting linear models to the transformed data of the form:

$$\ln(Y) = a + b \cdot \ln(M),$$

where *Y* is the phenotype of interest (i.e., normoxic $\dot{M}o_{2,Max}$, $\dot{M}o_{2,Standard}$, P_{crit}, ventricle dry mass, maximum enzyme activities, and hematocrit), *a* is a scaling factor (the standardized *Y* variable at 1 g of body mass, (Scheuffele et al. 2021)), *b* is the scaling exponent, and *M* is body mass. Models were fit using the "lm" function in the base *R* "stats" package (R Core Team 2020). After ensuring model assumptions of residual normality and homogeneity of variance were met, the statistical hypothesis for each linear model was tested using type 3 analysis of variance using the "Anova" function in the "car" package (Fox and Weisberg 2019).

To test the hypothesis that regulatory capacity for $\dot{M}o_{2,Max}$ in hypoxia declines with increasing body size, using the "lm" function in the base R "stats" package (R CoreTeam 2020), we fit a linear model of the form $R = c + dM$, where *R* is regulation value (%), *M* is body mass, and *c* and *d* are fitted constants. After ensuring model assumptions of residual normality and homoscedasticity were met, a type 3 ANOVA was used to determine whether mass significantly affected regulation value at $\alpha = 0.05$.

Results

Regression parameters and statistics for linear models of body mass vs. normoxic $\dot{M}o_{2,Max}$, $\dot{M}o_{2,Standard}$, gill surface area, S_{MMR}, S_{SMR}, P_{crit}, ventricle dry mass, and enzyme activities are reported in Table 1. The *S* ratio body mass

Table 1 Summary of allometric regression parameters for models of form $Y = aM^b$

Trait	*a* (±SE)	*b* (±SE)	R^2
MMR in normoxia	5.21 (±1.43)***	1.18 (±0.20)***	0.71
SMR	2.42 (±1.34)**	0.68 (±0.17)**	0.52
Gill surface area	567 (±1.8)***	0.93 (±0.17)*	0.34
S_{MMR}	85.3 (±1.8)***	− 0.17 (±0.32) [− 0.79, 0.47]	0.02
S_{SMR}	234 (±1.98)***	0.26 (±0.39) [− 0.51, 1.02]	0.03
P_{crit}	1.81 (±1.41)^{ns}	0.22(±0.20)^{ns}	0.08
Ventricle dry mass	0.066 (±1.42)***	1.22 (±0.20)***	0.75
COX (mg protein^{-1})	0.11 (±1.49)***	0.40 (±0.22)^{ns}	0.17
COX (g wet mass^{-1})	0.96 (±1.53)^{ns}	0.39 (±0.24)^{ns}	0.15
CS (mg protein^{-1})	0.12 (±1.50)*	− 0.17 (±0.23)^{ns}	0.03
CS (g wet mass^{-1})	0.29 (±1.43)**	− 0.15 (±0.20)^{ns}	0.04
COX (unit CS activity^{-1})^{A}	0.90 (±1.69)^{ns}	0.56 (±0.30)^{ns}	0.19
COX (unit CS activity^{-1})^{B}	3.32 (±1.71)*	0.54 (±0.30)^{ns}	0.17
LDH (mg protein^{-1})	29.3 (±1.35)***	0.26 (±0.17)^{ns}	0.14
LDH (g wet mass^{-1})	184 (±1)***	0.27 (±0.18)^{ns}	0.13

The regression parameter "*a*" and its standard error (SE) SE are back-transformed from the natural logarithm scale. 95% confidence intervals for slope estimates for *S* ratios are given in brackets [] and are calculated as SE × 1.96. Note that R^2 values are for the linear model on the natural logarithm transformed response and mass data

ns not significant

[A]Calculated based on protein-normalized enzyme activities

[B]Calculated based on protein-normalized enzyme activities

*$P \leq 0.05$

**$P \leq 0.01$

***$P \leq 0.001$

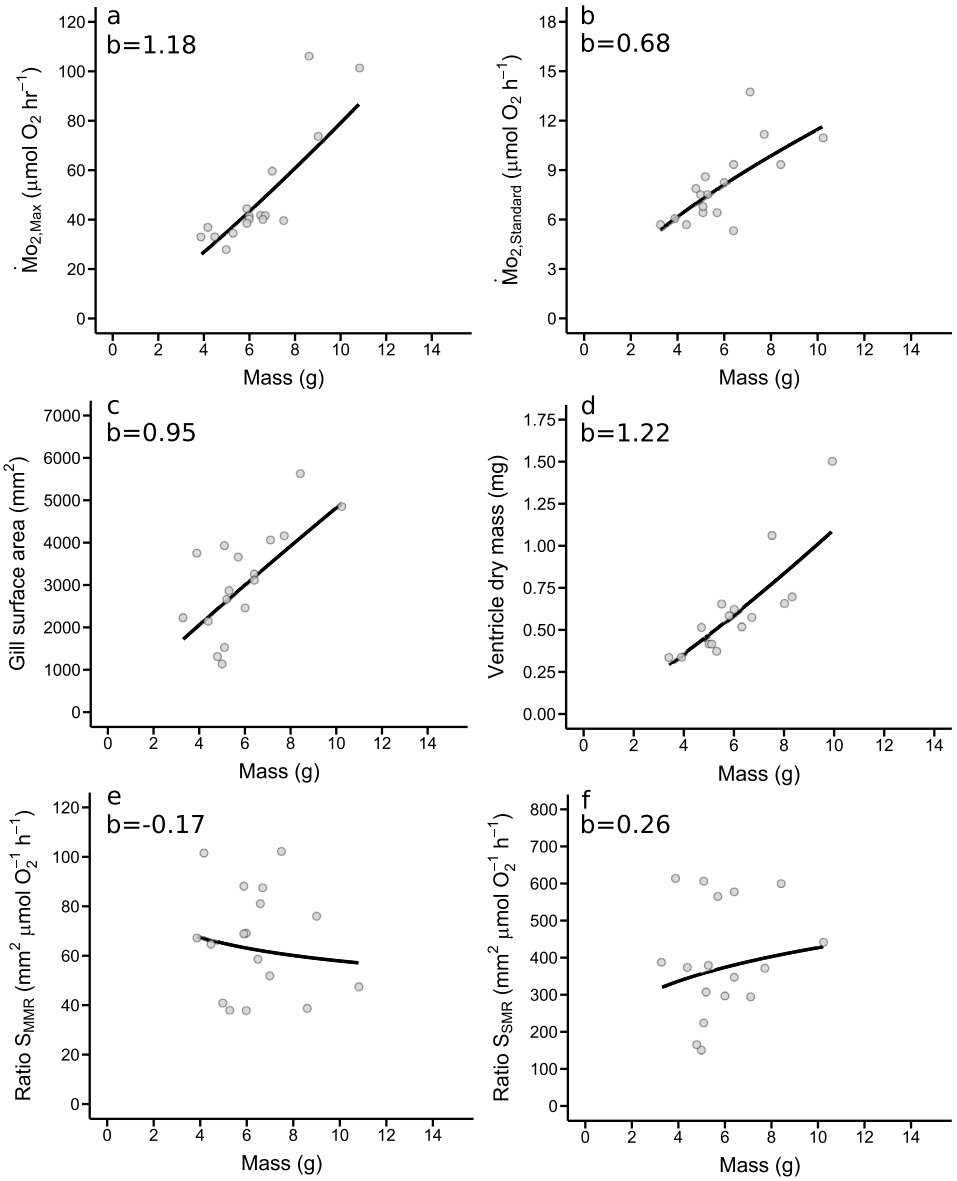

Fig. 1 The relationships between **a** $\dot{M}o_{2,Max}$ (µmol O_2 h^{-1}), **b** $\dot{M}o_{2,Standard}$ (µmol O_2 h^{-1}), **c** gill surface area (mm^2), **d** ventricle dry mass (mg), **e** the ratio of gill surface area to $\dot{M}o_{2,Max}$ (S_{MMR}), and **f** the ratio of gill surface area to $\dot{M}o_{2,Standard}$ (S_{SMR}). $N = 17$ in every panel except **d**, $N = 15$ for ventricle dry mass. The estimated scaling exponent b for each relationship is provided within each plot. Data are plotted with regressions fit to the natural-logarithm transformed body mass and physiological trait data. Plots of natural-logarithm transformed data and fitted linear regressions are provided in Fig. S7

scaling coefficients for $\dot{M}o_{2,Standard}$ (Table 1, $b_S = 0.26 \pm 0.39$ (95% CI), $R^2 = 0.03$) and $\dot{M}o_{2,Max}$ (Table 1, $b_S = -0.17 \pm 0.32$ (95% CI), $R^2 = 0.02$) were not significantly different from zero (Table 1).

Normoxic $\dot{M}o_{2,Max}$, $\dot{M}o_{2,Standard}$, gill surface area, and ventricle drymass (Fig. 1) significantly increased with body mass (Table 2). Body mass was not significantly related to P_{crit} (mean ± sem = 2.73 ± 0.14 kPA, Fig. S2), hematocrit (mean ± sem = 31 ± 1.3%, Fig. S3), or any of the metabolic enzymes assessed (Tables 2, 3, Fig. S4).

Although regulation value appeared to slightly decline with body mass, we did not detect a statistically significant change with mass ($F_{1,15} = 3.61$, $P = 0.08$, Fig. 2d). Two regulation values fell below 50%, one of which was more than 2 standard deviations below the mean, so after removing this low outlier the mean ± sem for the regulation value was 60 ± 2%, and the mean ± sem when including the outlier was 58 ± 2% (Fig. 2d).

Discussion

In contrast with the GOLH, we did not find evidence to support a limitation on maximum oxygen uptake capacity due to insufficient gill surface area. Although gill surface area scales slightly hypometrically with body mass ($b = 0.95$, Fig. 1), normoxic $\dot{M}o_{2,Max}$ scales hypermetrically ($b = 1.18$, Fig. 1). The body mass scaling exponent of S_{MMR}, an index of the gill surface area available to support maximum

Table 2 Type 3 ANOVA results for tests on linear models of body mass effects on traits

Trait	$F_{\text{Num df, Denom df}}$ for effect of ln(Mass)	P
MMR in normoxia	$F_{1,15}=36.4$	$\mathbf{2.3\times10^{-5}}$
SMR	$F_{1,15}=16.1$	**0.0011**
Gill surface area	$F_{1,15}=7.74$	**0.014**
S_{MMR}	$F_{1,15}=0.279$	0.60
S_{SMR}	$F_{1,15}=0.432$	0.52
P_{crit}	$F_{1,15}=1.31$	0.27
Ventricle dry mass	$F_{1,13}=6.12$	**0.028**
Hematocrit	$F_{1,15}=3.77$	0.071
COX (mg protein^{-1})	$F_{1,15}=3.12$	0.10
COX (g wet mass^{-1})	$F_{1,15}=2.61$	0.13
CS (mg protein^{-1})	$F_{1,15}=0.54$	0.48
CS (g wet mass^{-1})	$F_{1,15}=0.59$	0.45
COX (unit CS activity^{-1})[a]	$F_{1,15}=3.60$	0.08
COX (unit CS activity^{-1})[b]	$F_{1,15}=3.16$	0.10
LDH (mg protein^{-1})	$F_{1,15}=1.54$	0.15
LDH (g wet mass^{-1})	$F_{1,15}=2.27$	0.15

Bolded traits and P values indicate significant effects of body mass ($P \leq 0.05$)

[a]Based on protein-normalized activities

[b]Based on wet mass-normalized activities

Table 3 Summary of enzyme activity data

Enzyme	Unit	Mean ± SEM
Cytochrome C oxidase (COX)	mg protein^{-1}	0.23 ± 0.02
	g wet mass^{-1}	1.95 ± 0.49
	unit CS activity$^{-1,a}$	2.56 ± 0.22
	unit CS activity$^{-1,b}$	9.01 ± 0.71
Citrate synthase (CS)	mg protein^{-1}	0.09 ± 0.01
	g wet mass^{-1}	0.23 ± 0.05
Lactate dehydrogenase (LDH)	mg protein^{-1}	47 ± 2.3
	g wet mass^{-1}	302 ± 16

Cytochrome C oxidase: [a]based on protein-normalized activities, [b]based on wet mass-normalized activities

oxygen uptake rate, did not significantly differ from 0 ($b=-0.17\pm0.32$ (95% CI), $R^2=0.02$, Table 1). Likewise, since $\dot{M}o_{2,\text{Standard}}$ scales with an exponent ($b=0.68$, Fig. 1) much lower than gill surface area, it is unsurprising that S_{SMR} scales with an exponent that is also not significantly different from 0 ($b=0.26\pm0.39$ (95% CI), $R^2=0.03$, Table 1). Together these results suggest that, as in most other species analyzed using the S ratio approach to date (Scheuffele et al. 2021), *O. maculosus* possesses sufficient or more than sufficient gill surface area to meet minimum and maximum oxygen uptake demands across the full observed range of adult body masses in this species. These results indicate, consistent with the results of others suggesting distributed control of oxygen uptake and consumption (Darveau et al. 2002; Hochachka et al. 2003; Weibel and Hoppeler 2005; Glazier 2009; Killen et al. 2010; Hirst et al. 2014; Scheuffele et al. 2021; Norin 2022), that respiratory surface area allometry alone does not determine oxygen uptake capacity or its allometry.

Normoxic $\dot{M}o_{2,\text{Max}}$ appears to scale similarly to ventricle dry mass ($b=1.22$, Fig. 2), which could suggest an important role for heart size in setting the body mass allometry of tidepool sculpin normoxic $\dot{M}o_{2,\text{Max}}$. Ventricle size is a primary determinant of stroke volume and, therefore, an important determinant of cardiac output in fish (Farrell and Smith 2017), which in turn is an important determinant of $\dot{M}o_{2,\text{Max}}$ (Darveau et al. 2002; McArley et al. 2021; Weibel and Hoppeler 2005). Heart size generally scales linearly (i.e., $b=1$) with body mass in most fishes (Poupa and Lindström 1983; Farrell and Smith 2017), and we note that the hypermetric scaling exponent we obtained could be driven largely by the few large individuals with particularly high ventricle dry mass (Fig. 1d). The 95% CI for the ventricle dry mass scaling exponent includes $b=1.0$ (95% CI = [0.83, 1.61]), but the standard error of the estimated scaling exponent excludes $b=1.0$ ($b=1.22\pm0.20$, Table 1), suggesting that ventricle dry mass likely scales hypermetrically in *O. maculosus*, though this conclusion remains tentative. The potential functional significance of hypermetric heart size scaling remains unclear. Given that the GOLH is purported to functionally connect the scaling of gill surface area to metabolic capacity based on the similarity of their scaling relationships (Pauly 2021), the fact that ventricle dry mass scales much more closely with $\dot{M}o_{2,\text{Max}}$ than with gill surface area would suggest heart size may be a more important determinant of $\dot{M}o_{2,\text{Max}}$ than gill surface area. However, the degree of control heart size exerts over $\dot{M}o_{2,\text{Max}}$ in *O. maculosus* or other fish species, e.g., via control analysis, remains to be tested.

Consistent with previous analyses, we did not detect significant relationships between hematocrit and body mass. The hematocrit values in our study compared well with previous hematocrit measurements in *O. maculosus* (Current study: 31 ± 1.3%; Mandic et al. (2009): 35 ± 2%, data mean ± sem). Classic treatments suggest that hematocrit should not vary with body size because increasing hematocrit, which linearly increases oxygen carrying capacity in the blood, also increases the cost of blood convection due to increasing blood viscosity (Schmidt-Nielsen 1984; Calder 1996; Birchard 1997). However, at least within some range, fish are able to adjust hematocrit in response to changing oxygen demands or availability such as exercise, changing temperature, hypoxia, season, photoperiod, nutritional status, and toxin exposure (Gallaugher and Farrell 1998). Previous studies in fish have found empirical support for increases in hematocrit with body mass (Atkinson and Judd

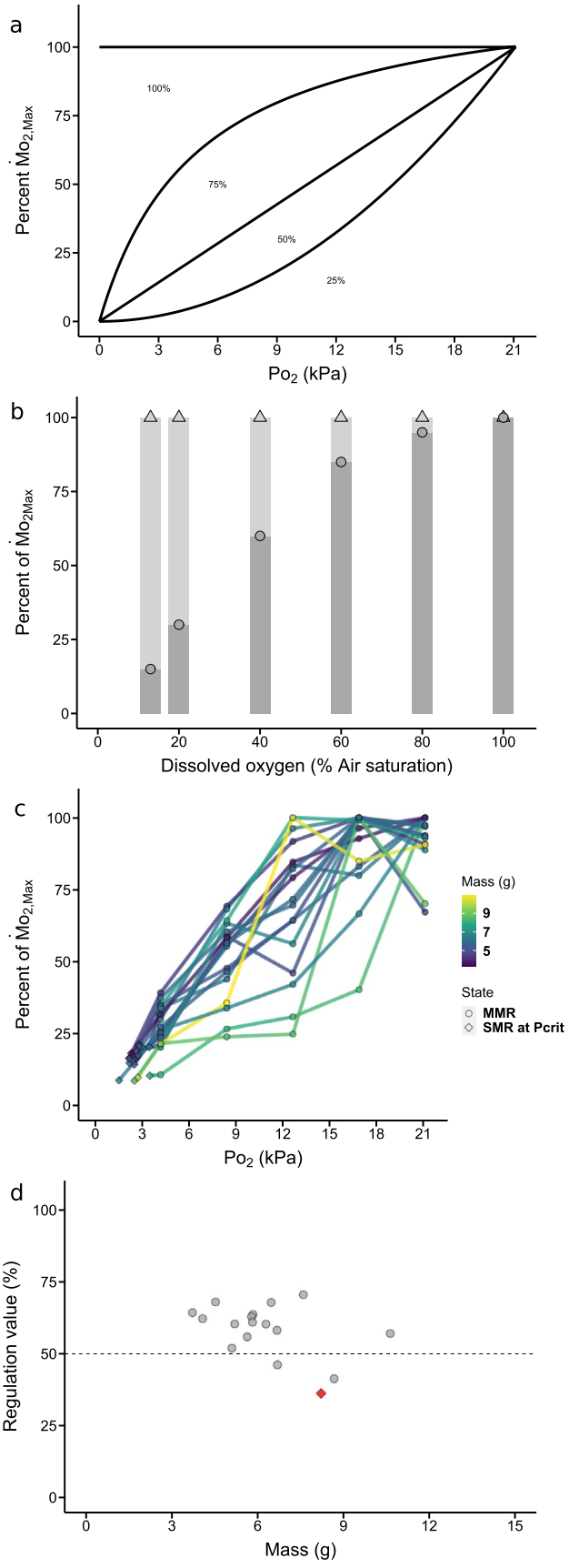

Fig. 2 **a** A schematic demonstrating the method of estimating regulatory capacity for $\dot{M}o_2$ in hypoxia using the regulation value of Alexander Jr and McMahon (2004). The regulation value R is the percentage of the area of the rectangle inscribed by a hypothetical perfect regulator, using data normalized to the empirically determined $\dot{M}o_{2,Max}$, by the experimentally obtained $\dot{M}o_2$ data in hypoxia. **b** Hypothetical example of the method of estimation of R used in the present study. The R value was calculated as $A_{Dark\ grey}/A_{Light\ grey} \times 100\%$, where $A_{Dark\ grey}$ represents the area inscribed by each experimentally determined $\dot{M}o_{2,Max}$ at each hypoxic Po_2 (i.e., 100% air saturation [air sat.], 80% air sat., 60% air sat., 40% air sat., 20% air sat., and P_{crit} for $\dot{M}o_{2,Standard}$) with an assumed width of 5% air sat., $A_{Light\ grey}$ represents the area for the hypothetical $\dot{M}o_{2,Max}$ at each Po_2, also with an assumed width of 5% air sat.. **c** $\dot{M}o_{2,Max}$ vs. Po_2 data plotted for each individual. Data are color-coded by body mass, and shape indicates whether a data point is an $\dot{M}o_{2,Max}$ estimate or P_{crit} for $\dot{M}o_{2,Standard}$. **d** Regulation value vs. body mass. The dotted horizontal line indicates the expected regulation value for an oxyconforming individual. The red diamond indicates a low outlier value based on the 2σ designation method

1978; Martínez et al. 1994; Altinok et al. 1998; Nespolo and Rosenmann 2002), but, as in our study, others have not (Vuren and Hattingh 1978; Beitinger et al. 1985; Clark and Farrell 2011). Although the relationship between hematocrit and body size bears further investigation, the lack of a relationship between these variables in *O. maculosus* suggests that, at least under common laboratory acclimation conditions, blood oxygen carrying capacity, indexed by hematocrit, is unlikely to play a significant role in limiting the oxygen uptake capacity of adult individuals of any size.

Although body mass frequently correlates with enzyme activities, we did not find any significant relationships between body mass and metabolic enzyme activities in white muscle in tidepool sculpins. In fish in general, mitochondrial enzyme activities such as citrate synthase (CS) and electron transport system enzymes including cytochrome c oxidase (COX) scale negatively with body mass, and glycolytic enzymes such as lactate dehydrogenase (LDH) scale positively with body mass, resulting in reciprocal intraspecific scaling relationships between oxidative and glycolytic enzyme activities (Moyes and LeMoine 2005). There are numerous exceptions to this pattern (Moyes and Genge 2010), and the origin and regulation of muscle enzyme metabolic scaling patterns remains an active area of investigation. Myonuclear domain, the volume of a muscle fiber serviced by a single nucleus, has been suggested to be an important regulator of mitochondrial content and could, therefore, be an important regulator of oxidative enzyme scaling patterns since myonuclear domain increases with increasing muscle fiber size and body size in fishes (Moyes and LeMoine 2005). The lack of a body mass relationship with CS activities, which provides an index of mitochondrial content, could suggest that over the range of body masses surveyed in our study myonuclear domain size is constant or sufficiently similar as to have myonuclear domain effects

subsumed under alternative regulatory mechanisms controlling enzyme expression levels. Incorporating DNA-content normalized estimates of enzyme activity into future analyses of oxidative enzyme capacity would be fruitful. In contrast with the situation in oxidative enzyme regulation studies, the foundation of scaling patterns (or lack thereof) in glycolytic enzyme activities under normoxic routine conditions is far from clear (Moyes and LeMoine 2005). GOLH suggests that tissue hypoxia occurs as a consequence of gill-derived oxygen uptake limitations as fish grow resulting in allometric fish growth (Pauly 2021). GOLH, therefore, predicts that under normoxic environmental conditions, fish tissues increasingly experience hypoxia as fish grow. This predicted relationship between size and degree of tissue hypoxia might be expected to produce a positive correlation between fish body mass and hypoxia inducible factor (HIF) activity in muscle given the role of hypoxia in regulating HIF activity in fish (Mandic et al. 2021; Pelster and Egg 2018). Whether HIF activity varies with body size in routine normoxic conditions and controls glycolytic metabolic programming in fish bears further investigation.

Most studies of the physiological basis of metabolic allometry rely on observational comparisons of scaling slopes at various levels of biological organization, but empirical manipulations are a powerful and necessary approach for determining the proximate basis of metabolic scaling patterns (Darveau et al. 2002; Hochachka et al. 2003; Glazier 2014; Harrison 2018; Norin 2022). Our empirical analysis of the effect of hypoxia on $\dot{M}o_{2,Max}$, based on the regulation value approach (Alexander Jr. and McMahon 2004), did not implicate an oxygen supply constraint on $\dot{M}o_{2,Max}$ with increasing body size (Fig. 2d). This result is consistent with the lack of a detectable relationship between P_{crit} and body mass in our study (Table 2) and by Mandic et al. (2009). Although there is debate over the physiological significance of P_{crit} (Wood 2018), P_{crit} is generally accepted as representing the Po_2 at which $\dot{M}o_{2,Max}$ equals $\dot{M}o_{2,Standard}$ and aerobic scope falls to nil (Claireaux and Chabot 2016; Regan et al. 2019; Seibel and Deutsch 2020; Seibel et al. 2021b; Verberk et al. 2022) and we have empirically supported this interpretation of P_{crit} in *O. maculosus* (Somo et al. 2022). Together the regulation value and P_{crit}—body mass analyses suggest that environmental hypoxia equally suppresses individual maximum oxygen uptake capacity irrespective of body size, at least in adult *O. maculosus*.

One possible alternative explanation for a limited relationship between gill surface area and respiratory capacity in *O. maculosus* is the possible contribution of respiratory surfaces other than the gill to oxygen uptake. Oxygen uptake at sites other than the gill have not been explicitly described in *O. maculosus*, but previous studies in several closely related intertidal species have found evidence for oxygen uptake at non-gill sites that improve air-breathing ability compared to subtidal congeners (Martin 1996). *O. maculosus* and other intertidal sculpins, like most marine air-breathing fishes (Graham 1997), do not have a dedicated air breathing organ, but despite this *O. maculosus* are capable of maintaining routine rates of respiratory gas exchange in moist air for several days without incurring an oxygen debt or lactate load (Sloman et al. 2008). Although intertidal sculpins generally have greater mass-specific gill surface area which supports increased oxygen uptake capacity in hypoxia (indexed by P_{crit}) compared to subtidal sculpins, *O. maculosus* have among the lowest mass-specific gill surface areas measured among these species (Mandic et al. 2009). Reduced gill surface area as well as reduced elaboration of the gill structures (shortened filaments, greater cartilage content) are traits thought to improve gill respiratory gas exchange in air by limiting structural gill collapse (Graham 1997; Martin 2014). How extra-gill sites of oxygen uptake contribute to oxygen uptake in marine fishes with changes in water oxygen content, exercise, or body size, remains poorly studied. A study in Pacific tarpon, one of two marine species with an air-breathing organ, found that oxygen uptake during high speed swimming in hypoxia is equally partitioned between the gills and air-breathing organ (Seymour et al. 2004). Whether gas exchange from sites besides the gills, such as the skin, especially under hypoxic conditions, could supplement oxygen uptake in hypoxia during recovery from exhaustive exercise, and how patterns of partitioning scale with body mass, remains to be studied in air-breathing fishes which lack air-breathing organs.

Although our combination of within-individual observational analyses across multiple aspects of the oxygen transport cascade and empirical test of the size-dependence of oxyregulatory capacity in *O. maculosus* constitutes a robust test of the GOLH, the relatively low total number of individuals in our study may limit the statistical power of our estimates of scaling exponents. We chose to follow Pauly's recommendation that tests of GOLH should use a body mass range that spans from 30% of maximum body size to as close to maximum body size as can be managed (Pauly 2021). This is important for avoiding possible confounding effects of changes in scaling relationships between juvenile and adult morphologies and physiologies (Pauly 2021), although the regulatory basis of changing allometric scaling relationships across life history states, for example in muscle metabolic enzymes, is of great interest (Norton et al. 2000; Moyes and LeMoine 2005; Moyes and Genge 2010). However, the frequency of individuals of larger body size generally decreases with size and age, often dramatically (Gibson and Yoshiyama 1999), greatly limiting their availability. Despite these constraints, our combined morphological and physiological analyses provide a robust first test of the GOLH as a mechanism structuring the size distribution of an intertidal fish. Future studies could extend the analyses

presented here to the smaller but abundant juvenile and young adult tidepool sculpins to determine whether there is evidence for changes in the scaling relationships assessed here during development and refine the estimates of scaling exponents obtained in our study.

Conclusions

In contrast with predictions from the GOLH, based on observational and empirical analyses of morphological and physiological relationships between body mass and oxygen uptake capacity, gill surface area, and other aspects of the oxygen transport cascade, we did not find support for either a gill surface area or general body-size associated limitation on oxygen uptake capacity in the tidepool sculpin, *O. maculosus*. Irrespective of body size, at least within adult fish, hypoxia equally suppresses maximum oxygen uptake capacity. The hypermetric scaling coefficient for ventricle dry mass ($b = 1.22$) suggests a potential role for the heart in setting the allometry of normoxic $\dot{M}o_{2,Max}$ ($b = 1.18$), though the functional significance of hypermetric scaling of the heart remains unclear. Whether other physiological traits, such as temperature tolerance, vary with size in *O. maculosus* as seen in other species (McKenzie et al. 2021) and subsequently contribute to the spatial distribution of this species is unknown but the allometries of respiratory capacity and gill surface area do not appear to be an important determinant of the spatial distribution of this species.

Supplementary Information The online version contains supplementary material available at https://doi.org/10.1007/s00360-023-01490-9.

Acknowledgements Thank you to Gigi Lau for providing tissue homogenization and enzyme analysis protocols and Hanna Scheuffele for helpful discussion of intraspecific allometric model fitting. Funding support was provided by a Natural Sciences and Engineering Research Council (NSERC) of Canada Discovery Grant to JGR. DAS was supported by The University of British Columbia Graduate Four Year Fellowship.

Author contributions Conceptualization: [DAS, JGR]; methodology: [DAS, JGR]; formal analysis and investigation: [DAS, KC]; writing—original draft preparation: [DAS]; writing—review and editing: [DAS, JGR]; funding acquisition: [JGR]; supervision: [JGR].

Data availability statement The raw data generated during the current study and R code used to produce figures and analyses are available in the FigShare repository: [https://figshare.com/projects/Supplementary_material_from_Gill_surface_area_allometry_does_not_constrain_the_body_mass_scaling_of_maximum_oxygen_uptake_rate_in_the_tidepool_sculpin_Oligocottus_maculosus_/142235].

Declarations

Conflict of interests The authors have no relevant financial or non-financial interests to disclose.

Ethics statement All experimental procedures were approved by the UBC Animal Care Committee (A17-0293). Fish collections were approved by the Department of Fisheries and Oceans Canada (scientific license XR 239 2017) and conducted under Huu-Ay-Aht Heritage Investigations permit HFN 2017-027.

References

Alexander JE Jr, McMahon RF (2004) Respiratory response to temperature and hypoxia in the zebra mussel Dreissena polymorpha. Comp Biochem Physiol A Mol Integr Physiol 137:425–434. https://doi.org/10.1016/j.cbpb.2003.11.003

Altinok I, Galli SM, Chapman FA (1998) Ionic and osmotic regulation capabilities of juvenile Gulf of Mexico sturgeon, *Acipenser oxyrinchus de sotoi*. Comp Biochem Physiol A Mol Integr Physiol 120:609–616

Atkinson E, Judd FW (1978) Comparative hematology of *Lepomis microlophus* and *Cichlasoma cyanoguttatum*. Copeia 1978:230–237

Beitinger T, Pettit M, Hutchinson V (1985) Oxygen transfer characteristics of the blood of reedfish, *Erpetoichthys calabaricus*. Comp Biochem Physiol 82A:553–558

Birchard GF (1997) Optimal hematocrit: theory, regulation, and implications. Am Zool 37:65–72

Bradford MM (1976) A rapid and sensitive method for the quantitation of microgram quantities of protein utilizing the principle of protein-dye binding. Anal Biochem 72:248–254

Calder WA III (1996) Size, function, and life history. Dover Publications Inc, Mineola

Chabot D (2020) fishMO_2: calculate and plot the standard metabolic rate (SMR), the critical oxygen level (O_2crit) and the specific dynamic action (SDA) and related variables in fishes and crustaceans. https://www.researchgate.net/project/fishMO2-a-R-package-to-calculate-and-plot-SMR-O2crit-and-SDA. Accessed 4 Mar 2021

Chabot D, Steffensen JF, Farrell AP (2016) The determination of standard metabolic rate in fishes. J Fish Biol 88:81–121. https://doi.org/10.1111/jfb.12845

Cheung WWL, Pauly D (2016) Impacts and effects of ocean warming on marine fishes. In: Laffoley D, Baxter J (eds) Explaining ocean warming: causes, scale, effects and consequences. International Union for Conservation of Nature (IUCN), Gland, pp 239–253

Cheung WWL, Sarmiento JL, Dunne J et al (2013) Shrinking of fishes exacerbates impacts of global ocean changes on marine ecosystems. Nat Clim Change 3:254–258. https://doi.org/10.1038/nclimate1691

Christoffersen B (2019) rollRegres: fast rolling regression and expanding window linear regression. Version 0.1.3. https://CRAN.R-project.org/package=rollRegres. Accessed 4 Mar 2022

Claireaux G, Chabot D (2016) Responses by fishes to environmental hypoxia: integration through Fry's concept of aerobic metabolic scope. J Fish Biol 88:232–251. https://doi.org/10.1111/jfb.12833

Clark TD, Farrell AP (2011) Effects of body mass on physiological and anatomical parameters of mature salmon: evidence against a universal heart rate scaling exponent. J Exp Biol 214:887–893. https://doi.org/10.1242/jeb.051607

Clarke A (ed) (2017) Metabolism. In: Principles of thermal ecology. Oxford University Press, Oxford, pp 163–195

Darveau C-A, Suarez RK, Andrews RD, Hochachka PW (2002) Allometric cascade as a unifying principle of body mass effects on metabolism. Nature 417:166–170. https://doi.org/10.1038/417166a

Ern R (2019) A mechanistic oxygen- and temperature-limited metabolic niche framework. Philos Trans R Soc B Biol Sci 374:20180540. https://doi.org/10.1098/rstb.2018.0540

Farrell AP, Richards JG (2009) Defining hypoxia: an integrative synthesis of the responses of fish to hypoxia. In: Richards JG, Farrell AP, Brauner CJ (eds) Hypoxia. Academic Press, London, pp 487–503

Farrell AP, Smith F (2017) Cardiac form, function and physiology. In: Gamperl AK, Gillis TE, Farrell AP, Brauner CJ (eds) The cardiovascular system: morphology, control and function. Elsevier, Cambridge, pp 155–264

Farrell AP, Mueller CA, Seymour RS (2021) Coming up for air. J Exp Biol. https://doi.org/10.1242/jeb.243101

Fox J, Weisberg S (2019) An R companion to applied regression, 3rd edn. Sage, Thousand Oaks CA

Froese R, Pauly D (2021) FishBase. www.fishbase.org. Accessed 7 Jan 2023

Gallaugher P, Farrell AP (1998) Hematocrit and blood oxygen-carrying capacity. In: Perry SF, Tufts BL (eds) Fish respiration. Academic Press, San Diego

Gattuso J-P, Magnan A, Bille R et al (2015) Contrasting futures for ocean and society from different anthropogenic CO_2 emissions scenarios. Science 349:aac4722. https://doi.org/10.1126/science.aac4722

Gibson RN, Yoshiyama RM (1999) Intertidal fish communities. In: Horn MH, Martin KLM, Chotkowski MA (eds) Intertidal fishes: life in two worlds. Academic Press, San Diego, pp 264–296

Glazier DS (2009) Activity affects intraspecific body-size scaling of metabolic rate in ectothermic animals. J Comp Physiol B Biochem Syst Environ Physiol 179:821–828. https://doi.org/10.1007/s00360-009-0363-3

Glazier D (2014) Metabolic scaling in complex living systems. Systems 2:451–540. https://doi.org/10.3390/systems2040451

Graham JB (1997) Air breathing fishes: evolution, diversity, and adaptation. Academic Press, San Diego

Harrison JF (2018) Approaches for testing hypotheses for the hypometric scaling of aerobic metabolic rate in animals. Am J Physiol Regul Integr Comp Physiol 315:R879–R894. https://doi.org/10.1152/ajpregu.00165.2018

Henriksson P, Mandic M, Richards JG (2008) The osmorespiratory compromise in sculpins: impaired gas exchange is associated with freshwater tolerance. Physiol Biochem Zool 81:310–319. https://doi.org/10.1086/587092

Hirst AG, Glazier DS, Atkinson D (2014) Body shape shifting during growth permits tests that distinguish between competing geometric theories of metabolic scaling. Ecol Lett 17:1274–1281. https://doi.org/10.1111/ele.12334

Hochachka PW, Darveau C-A, Andrews RD, Suarez RK (2003) Allometric cascade: a model for resolving body mass effects on metabolism. Comp Biochem Physiol A Mol Integr Physiol 134:675–691. https://doi.org/10.1016/s1095-6433(02)00364-1

Karnovsky MJ (1965) A formaldehyde-glutaraldehyde fixative of high osmolality for use in electron microscopy. J Cell Biol 27:137A

Killen SS, Atkinson D, Glazier DS (2010) The intraspecific scaling of metabolic rate with body mass in fishes depends on lifestyle and temperature. Ecol Lett 13:184–193. https://doi.org/10.1111/j.1461-0248.2009.01415.x

Killen SS, Christensen EAF, Cortese D et al (2021) Guidelines for reporting methods to estimate metabolic rates by aquatic intermittent-flow respirometry. J Exp Biol 224:jeb242522. https://doi.org/10.1242/jeb.242522

Lefevre S, McKenzie DJ, Nilsson GE (2017) Models projecting the fate of fish populations under climate change need to be based on valid physiological mechanisms. Glob Change Biol 23:3449–3459. https://doi.org/10.1111/gcb.13652

Lefevre S, McKenzie DJ, Nilsson GE (2018) In modelling effects of global warming, invalid assumptions lead to unrealistic projections. Glob Change Biol 24:553–556. https://doi.org/10.1111/gcb.13978

Lefevre S, Wang T, McKenzie DJ (2021) The role of mechanistic physiology in investigating impacts of global warming on fishes. J Exp Biol 224:jeb238840. https://doi.org/10.1242/jeb.238840

Mandic M, Todgham AE, Richards JG (2009) Mechanisms and evolution of hypoxia tolerance in fish. Proc R Soc B Biol Sci 276:735–744. https://doi.org/10.1098/rspb.2008.1235

Mandic M, Joyce W, Perry SF (2021) The evolutionary and physiological significance of the Hif pathway in teleost fishes. J Exp Biol 224:jeb231936. https://doi.org/10.1242/jeb.231936

Martin KLM (1996) An ecological gradient in the air-breathing ability among marine Cottid fishes. Physiol Zool 69:1096–1113

Martin KLM (2014) Theme and variations: amphibious air-breathing intertidal fishes. J Fish Biol 84:577–602. https://doi.org/10.1111/jfb.12270

Martínez FJ, García-Riera MP, Canteras M et al (1994) Blood parameters in rainbow trout (*Oncorhynchus mykiss*): simultaneous influence of various factors. Comp Biochem Phyisol 107A:95–100

McArley TJ, Morgenroth D, Zena LA, Ekström AT, Sandblom E (2021) Normoxic limitation of maximal oxygen consumption rate, aerobic scope and cardiac performance in exhaustively exercised rainbow trout (*Onchorhynchus mykiss*). J Exp Biol 224:jeb242614. https://doi.org/10.1242/jeb.242614

McKenzie DJ, Zhang Y, Eliason EJ et al (2021) Intraspecific variation in tolerance of warming in fishes. J Fish Biol 98:1536–1555. https://doi.org/10.1111/jfb.14620

Metaxas A, Scheibling RE (1993) Community structure and organization of tidepools. Mar Ecol Prog Ser 98:187–198

Moyes CD, Genge CE (2010) Scaling of muscle metabolic enzymes: an historical perspective. Comp Biochem Physiol A Mol Integr Physiol 156:344–350. https://doi.org/10.1016/j.cbpa.2010.01.025

Moyes CD, LeMoine CMR (2005) Control of muscle bioenergetic gene expression: implications for allometric scaling relationships of glycolytic and oxidative enzymes. J Exp Biol 208:1601–1610. https://doi.org/10.1242/jeb.01502

Mueller CA, Seymour RS (2011) The regulation index: a new method for assessing the relationship between oxygen consumption and environmental oxygen. Physiol Biochem Zool 84:522–532. https://doi.org/10.1086/661953

Nakamura R (1976) Temperature and the vertical distribution of two tidepool fishes (*Oligocottus maculosus*, *O. snyderi*). Copeia 1976:143–152

Nespolo RF, Rosenmann M (2002) Intraspecific allometry of haematological parameters in *Basilichthys australis*. J Fish Biol 60:1358–1362. https://doi.org/10.1006/jfbi.2002.1949

Norin T (2022) Growth and mortality as causes of variation in metabolic scaling among taxa and taxon levels. Integr Comp Biol. https://doi.org/10.1093/icb/icac038

Norton SF, Eppley ZA, Sidell BD (2000) Allometric scaling of maximal enzyme activities in the axial musculature of striped bass, *Morone saxatilis* (Walbaum). Physiol Biochem Zool 73:819–828

Pauly D (2021) The gill-oxygen limitation theory (GOLT) and its critics. Sci Adv 7:eabc6050. https://doi.org/10.1126/sciadv.abc6050

Pauly D, Cheung WWL (2018a) On confusing cause and effect in the oxygen limitation of fish. Glob Change Biol 24:e743–e744. https://doi.org/10.1111/gcb.14383

Pauly D, Cheung WWL (2018b) Sound physiological knowledge and principles in modeling shrinking of fishes under climate change. Glob Change Biol 24:e15–e26. https://doi.org/10.1111/gcb.13831

Pelster B, Egg M (2018) Hypoxia-inducible transcription factors in fish: expression, function and interconnection with the circadian clock. J Exp Biol 221:jeb163709. https://doi.org/10.1242/jeb163709

Phuong LM, Damsgaard C, Huong DTT, Ishimatsu A, Wang T, Bayley M (2017) Recovery of blood gases and haematological parameters upon anaesthesia with benzocaine, MS-222 or Aqui-S in the air-breathing catfish *Pangasianodon hypophthalmus*. Ichtyol Res 64:84–92. https://doi.org/10.1007/s10228-016-0545-4

Pörtner H-O (2021) Climate impacts on organisms, ecosystems and human societies: integrating OCLTT into a wider context. J Exp Biol 224:jeb238360. https://doi.org/10.1242/jeb.238360

Poupa O, Lindtröm L (1983) Comparative and scaling aspects of heart and body weights with reference to blood supply of cardiac fibers. Comp Biochem Physiol 76:413–421

Prinzing TS, Zhang Y, Wegner NC, Dulvy NK (2021) Analytical methods matter too: establishing a framework for estimating maximum metabolic rate for fishes. Ecol Evol 00:1–17. https://doi.org/10.1002/ece3.7732

R Core Team (2020) R: a language and environment for statistical computing. R Foundation for Statistical Computing, Vienna

Regan MD, Mandic M, Dhillon RS et al (2019) Don't throw the fish out with the respirometry water. J Exp Biol 222:jeb.200253. https://doi.org/10.1242/jeb.200253

Richards JG (2011) Physiological, behavioral and biochemical adaptations of intertidal fishes to hypoxia. J Exp Biol 214:191–199. https://doi.org/10.1242/jeb.047951

Rodgers EM (2021) Adding climate change to the mix: responses of aquatic ectotherms to the combined effects of eutrophication and warming. Biol Lett 17:20210442. https://doi.org/10.1098/rsbl.2021.0442

Scheuffele H, Jutfelt F, Clark TD (2021) Investigating the gill-oxygen limitation hypothesis in fishes: intraspecific scaling relationships of metabolic rate and gill surface area. Conserv Physiol. https://doi.org/10.1093/conphys/coab040

Schmidt-Nielsen K (1984) Scaling: why is animal size so important? Cambridge University Press, Cambridge

Seibel BA, Deutsch C (2020) Oxygen supply capacity in animals evolves to meet maximum demand at the current oxygen partial pressure regardless of size or temperature. J Exp Biol 223:jeb210492. https://doi.org/10.1242/jeb.210492

Seibel B, Andres A, Birk M et al (2021a) Response to "Coming up for air." J Exp Biol 224:jeb.243148. https://doi.org/10.1242/jeb.243148

Seibel BA, Andres A, Birk MA et al (2021b) Oxygen supply capacity breathes new life into the critical oxygen partial pressure (P_{crit}). J Exp Biol 224:jeb.242210. https://doi.org/10.1242/jeb.242210

Seymour RS, Christian K, Bennett MB et al (2004) Partitioning respiration between the gills and air-breathing organ in response to aquatic hypoxia and exercise in the pacific tarpon, *Megalops cyprinoides*. Physiol Biochem Zool 77:760–767

Sloman KA, Mandic M, Todgham AE et al (2008) The response of the tidepool sculpin, *Oligocottus maculosus*, to hypoxia in laboratory, mesocosm and field environments. Comp Biochem Physiol A Mol Integr Physiol 149:284–292. https://doi.org/10.1016/j.cbpa.2008.01.004

Soivio A, Nyholm K, Huhti M (1977) Effects of anaesthesia with MS-222, neutralized MS-222 and benzocaine on the blood constituents of rainbow trout, Salmo gairdneri. J Fish Biol 10:91–101. https://doi.org/10.1111/j.1095-8649.1977.tb04045.x

Somo DA, Chu K, Richards JG (2022) Aerobic scope falls to nil at P_{crit} and anaerobic ATP production increases below P_{crit} in the tidepool sculpin, *Oligocottus maculosus*. Biol Lett 18:20220342. https://doi.org/10.1098/rsbl.2022.0342

Truchot J-P, Duhamel-Jouve A (1980) Oxygen and carbon dioxide in the marine intertidal environment: diurnal and tidal changes in rockpools. Respir Physiol 39:241–254

van Vuren JHJ, Hattingh J (1978) A seasonal study of the haematology of wild freshwater fish. J Fish Biol 13:305–313

Verberk WCEP, Sandker JF, van de Pol ILE, Urbina MA, Wilson RW, McKenzie DJ, Leiva FP (2022) Body mass and cell size shape the tolerance of fishes to low oxygen in a temperature-dependent manner. Glob Change Biol 00:1–13. https://doi.org/10.1111/gcb.16319

Weibel ER, Hoppeler H (2005) Exercise-induced maximal metabolic rate scales with muscle aerobic capacity. J Exp Biol 208:1635–1644. https://doi.org/10.1242/jeb.01548

Wood CM (2018) The fallacy of the P_{crit}—are there more useful alternatives? J Exp Biol 221:jeb163717. https://doi.org/10.1242/jeb.163717

Wuitchik SJS, Harder LD, Meschkat CA, Rogers SM (2018) Physical tidepool characteristics affect age- and size-class distributions and site fidelity in tidepool sculpin (*Oligocottus maculosus*). Can J Zool 96:1326–1335. https://doi.org/10.1139/cjz-2017-0297

Zander CD, Nieder J, Martin KL (1999) Vertical distribution patterns. In: Horn MH, Martin KL, Chotkowski MA (eds) Intertidal fishes: life in two worlds. Academic Press, London, pp 26–53

Zhang Y, Montgomery DW, White CF et al (2022) Characterizing the hypoxic performance of a fish using a new metric: PAAS-50. J Exp Biol 225:jeb.244239. https://doi.org/10.1242/jeb.244239